Published online 23 January 2017

Nucleic Acids Research, 2017, Vol. 45, No. 9 ***5375–5386***
doi: 10.1093/nar/gkx016

Ligand binding to 2′-deoxyguanosine sensing riboswitch in metabolic context

Yong-Boum Kim[1], Anna Wacker[1], Karl von Laer[2], Vladimir V. Rogov[3], Beatrix Suess[2] and Harald Schwalbe[1,*]

[1]Institute for Organic Chemistry and Chemical Biology, Center for Biomolecular Magnetic Resonance, Johann Wolfgang Goethe-University, Max-von-Laue-Str. 7, D-60438 Frankfurt/Main, Germany, [2]Department of Biology, Technical University Darmstadt, Schnittspahnstr. 10, 64287 Darmstadt, Germany and [3]Institute of Biophysical Chemistry and Center for Biomolecular Magnetic Resonance, Johann Wolfgang Goethe University, Max-von-Laue-Str. 9, 60438 Frankfurt/Main, Germany

Received November 11, 2016; Revised December 16, 2016; Editorial Decision December 22, 2016; Accepted January 04, 2017

ABSTRACT

The *mfl*-riboswitch is a transcriptional off-switch, which down-regulates expression of subunit β of ribonucleotide reductase in *Mesoplasma florum* upon 2′-deoxyguanosine binding. We characterized binding of 2′-deoxyguanosine to the *mfl*-aptamer domain (WT aptamer) and a sequence-stabilized aptamer (MT aptamer) under *in vitro* and 'in-cell-like' conditions by isothermal titration calorimetry (ITC) and nuclear magnetic resonance (NMR) spectroscopy. 'In-cell-like' environment was simulated by *Bacillus subtilis* cell extract, in which both aptamers remained sufficiently stable to detect the resonances of structural elements and ligand binding in 2D NMR experiments. Under 'in-cell-like'-environment, (i) the WT aptamer bound the endogenous metabolite guanosine and (ii) 2′-deoxyguanosine efficiently displaced guanosine from the WT aptamer. In contrast, MT aptamer exhibited moderate binding to 2′-deoxyguanosine and weak binding to guanosine. NMR experiments indicated that binding of guanosine was not limited to the aptamer domain of the riboswitch but also the full-length *mfl*-riboswitch bound guanosine, impacting on the regulation efficiency of the riboswitch and hinting that, in addition to 2′-deoxyguanosine, guanosine plays a role in riboswitch function *in vivo*. Reporter gene assays in *B. subtilis* demonstrated the regulation capacity of the WT aptamer, whereas the MT aptamer with lower affinity to 2′-deoxyguanosine was not able to regulate gene expression.

INTRODUCTION

RNA regulation sequences are becoming popular targets for therapeutical purposes and a utility model for synthetic biology. Riboswitches are *cis*-acting RNA elements, commonly residing in the 5′-untranslated region of prokaryotic mRNAs that specifically bind metabolites and directly regulate the downstream gene expression by undergoing allosteric changes upon ligand binding (1–3).

Synthetic biology aims at exploiting the specific features of riboswitches, namely ligand binding with high specificity and affinity, non-toxicity and high stability to engineer biosensors or exogenous synthetic gene regulators. SELEX (Systematic Evolution of Ligands by EXponential Enrichment) is an *in vitro* method to evolve such synthetic aptamers to a specific target molecule by iterative partitioning and amplification of binding-competent RNA sequences (4,5). The resulting RNA sequences are promising candidates as functional tools, but often fail to carry out their desired function *in vivo* (6).

In this context, we investigate here two RNA aptamers both *in vitro* and *in vivo* to illustrate that (i) engineering approaches to obtain synthetic riboswitches should consider the composition of the host-metabolome and (ii) structure biological optimization of RNA sequences e.g. towards stability and conformational homogeneity can have dramatic consequences for function.

We investigated two RNA aptamers, the aptamer domain of the class IA 2′-deoxyguanosine (2′dG) riboswitch (WT, Figure 1 A) from *M. florum* and its sequence-stabilized aptamer derivative (mutant = MT aptamer, Figure 1B) by *in vitro* and 'in-cell-like' NMR spectroscopy. In contrast to true 'in-cell NMR spectroscopy', where samples inside live cells are monitored, we use cell extracts to mimick the live environment but avoid limitations of sample concentration. Previous studies showed that MT aptamer binds ligand in a very similar manner compared to the WT (7,8). 2′dG spe-

*To whom correspondence should be addressed. Tel: +49 69 79829737; Fax: +49 69 79829515; Email: Schwalbe@nmr.uni-frankfurt.de

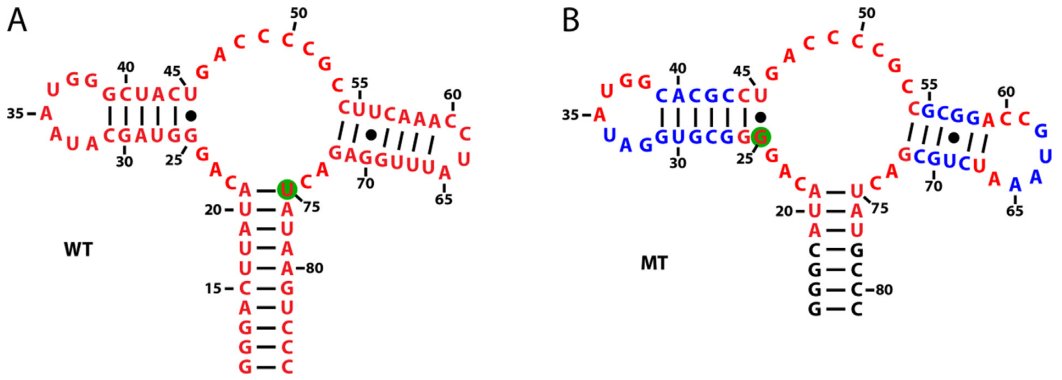

Figure 1. Secondary structures of WT *mfl*-aptamer (**A**) and MT aptamer (**B**). Ligand binding pocket (comprising nucleotides AUACAGGG-CUGACCCC GCC-GACUAU) and the nucleotides involved in the long-distance loop-loop-interaction (nucleotides AUGG-ACC) are identical with the WT sequence (labeled with red letters). The nucleotides colored in blue are secondary structure-stabilizing mutations derived from the guanine-sensing riboswitch of *B. subtilis*. Green circled nucleotides are the ligand binding reporter signals we have detected in 2D-NMR experiments (U75 for WT, G25 for MT aptamer). Nucleotide numbering is based on the purine aptamer nomenclature (23).

cific purine riboswitches have only been found in *M. florum*. The class IA riboswitch is located upstream of the gene encoding the ribonucleotide reductase subunit β. This enzyme carries out the conversion of phosphorylated ribonucleotides to their corresponding phosphorylated deoxyribonucleotides, the building blocks of DNA (9,10). Thus, it represents the only 2′-dG specific binding pocket known up to now, and hence is an exclusive member within the metabolite binding boxes in the toolbox of synthetic biology. MT aptamer design was guided by our experiences with the good properties for structural biology studies of the guanine-sensing *xpt-pbuX*-aptamer (11) and the observation of highly conserved secondary structure of aptamers among the mesoplasma family of riboswitches and the previously described purine-sensing riboswitches (7). By a similar approach, the binding mode of the 2′-dG aptamer was elucidated by crystallography using a construct where the 2′-dG aptamer binding pocket nucleotides were systematically embedded into the *xpt-pbuX* aptamer frame (12).

For both the functional studies in live cells and ligand binding NMR experiments in-cell-like environment, we utilized *B. subtilis* cells and cell extracts, respectively. Since *M. florum* has evolved from Gram positive bacteria, it is phylogenetically closer to *B. subtilis* than e.g. to *Escherichia coli*. To have a direct comparison between both aptamers in NMR experiments with regard to structure formation, stability and ligand binding, WT and MT aptamer were labeled with different sets of ^{15}N-ribonucleotides. Thus, the WT and MT aptamers could be investigated in the identical experiment to allow rigorous testing of the effect of different environments including *in vitro* buffer, in-cell extract and in metabolite extract. The NMR experiments carried out in-cell extract have previously been shown to be an alternative to in-cell NMR, as the cell extract contains all macromolecules, in particular also RNases, endogenous metabolites and other compounds, adding to the viscosity and mimicking molecular crowding (13,14).

Both aptamers were slowly degraded in-cell extract over time, but their stability was sufficiently high to allow us to record 2D experiments. The NMR spectra recorded in-cell extract exhibited differences to the *in vitro* spectrum, particularly with respect to ligand binding. ITC results from both aptamers *in vitro* and in metabolite extract indicated that ligand binds to WT more tightly and could displace pre-bound endogenous metabolites. In further experiments, we could show that the abundant metabolite guanosine, but not guanosine-monophosphate or guanosine-triphosphate competed for binding to the WT aptamer domain as well as to the full-length form of the riboswitch.

MATERIALS AND METHODS

RNA preparation

^{15}N-labeled nucleotides for *in vitro* transcription were purchased from Silantes (Munich). Non-labeled nucleotides were purchased from Sigma (Munich). Both nucleotides were used without further purification. The wild-type and the sequence-modified RNA aptamers were prepared by *in vitro* transcription from linearized plasmids using T7-polymerase as described (15). RNA concentrations were determined by UV spectroscopy with an extinction coefficient of 635×10^3 M^{-1} cm^{-1} at 260 nm for the wild-type RNA aptamer and 663×10^3 M^{-1} cm^{-1} for the sequence-modified RNA aptamer. Each RNA oligonucleotide was refolded into a homogeneous conformation by thermal denaturation of the RNA at high concentration (0.2–0.5 mM) followed by dilution to 0.05 mM and rapid cooling on ice. RNA samples were freeze-dried and exchanged into NMR-buffer (25 mM potassium phosphate, 50 mM potassium chloride, $MgCl_2$ according to desired final Mg^{2+} concentration, at pH 6.2), into *B. subtilis* cell extract or metabolite extract in buffer containing 50 mM potassium hydrogen phosphate, 50 mM potassium chloride, 5 mM magnesium chloride, pH 6.2. Conformational homogeneity of all samples was confirmed by native polyacrylamide gel electrophoresis. The RNA-ligand complex for the wild-type RNA aptamer was prepared at 2-fold molar excess of ligand over RNA. The RNA-ligand complex for the sequence-modified RNA aptamer was prepared by further addition of up to 8-fold molar excess of $MgCl_2$ over RNA. Ligand concentration was determined by UV/Vis spectroscopy using a molar extinction coefficient of 13.3×10^3 M^{-1} cm^{-1} at 254 nm.

NMR spectroscopy

NMR spectra were recorded at 600, 700 and 800 MHz Bruker spectrometers equipped with cryogenic probes and z-axis gradient systems. Pseudo 3D ^{1}H,^{15}N-BEST-TROSY spectra (16,17) were recorded at 600 MHz with optimized parameters, 2.53 ms PC9-pulse (18) centered at 11.5 ppm for imino proton excitation, a 1.73 ms Reburp refocusing pulse (19) and a 1.53 ms Eburp excitation and time-reversed Eburp2tr flip-back pulse (17). 2042 × 144 complex points were acquired in the direct and the indirect dimension, respectively, with four scans per point. All experiments were conducted at 291 K.

For the titration experiments, both 1D ^{14}N-edited and ^{15}N-edited imino proton spectra were recorded after each titration with unlabeled 2′-deoxyguanosine to ^{15}N-labeled aptamer probe. All spectra were recorded at a 600 MHz spectrometer with 256 scans at 291 K.

Preparation of *B. subtilis* cell extract

LB medium inoculated with *B. subtilis* was incubated at 37°C for 16 h to OD_{600} = 1.6–1.8. The cells were harvested by centrifugation at 4°C with 4000 rpm for 15 min (Beckman Coulter Avanti JXN-26, JLA-8.1000). The weight of the wet cell pellet was determined in order to reconstitute the freeze-dried cell extract in same amount of water after finished lysis. The harvested cell pellet was resuspended in 100 ml water and lysed in Microfluidizer (Microfluidics M-110P). The cell lysate was freeze-dried and resuspended in water or NMR-buffer, respectively.

Preparation of *B. subtilis* metabolite extract

LB medium inoculated with *B. subtilis* was incubated at 37°C for 16 h to OD_{600} = 1.6–1.8. The cells were harvested by centrifugation at 4°C with 4000 rpm for 15 min (Beckman Coulter Avanti JXN-26, JLA-8.1000). The cell pellet was washed with PBS buffer twice to remove residuals of LB medium. The weight of the wet cell pellet was determined and 10 ml/g extraction solution (acetonitrile:methanol:water, 2:2:1) was added and thoroughly mixed. Shock freezing in liquid nitrogen, thawing and thorough mixing of the cell suspension was repeated thrice. The extraction solution is responsible for quenching and isolation of the cells to extract the metabolites. Subsequently six cycles of sonication (30 s, 5 × 10%, power level 70, 30 s break) were carried out to further disrupt the cell wall and macromolecules to isolate them from metabolites. After centrifugation of the cell lysate (10 000 × g, 4°C, 20 min) to remove cell debris the supernatant was transferred into a new tube. After freeze-drying the powder of metabolites was resuspended in water or NMR-buffer, respectively.

Isothermal titration calorimetry (ITC)

For all but one titration experiment a MicroCal iTC200 (Malvern Instruments) was used. For the displacement experiment a VP-ITC calorimeter was used. All experiments were performed at 18°C using freeze-dried aptamer and ligand resuspended either in buffer containing 50 mM potassium hydrogen phosphate, 50 mM potassium chloride, 5 mM magnesium chloride, pH 6.2 or in metabolite extract in buffer containing 50 mM potassium hydrogen phosphate, 50 mM potassium chloride, 5 mM magnesium chloride, pH 6.2. The following samples were prepared: WT aptamer *in vitro*: 572 μM 2′-deoxyguanosine was titrated into 48 μM WT aptamer solution in 25 steps. WT aptamer *in metabolo*: 424 μM 2′-deoxyguanosine was titrated into 44 μM WT aptamer solution in 20 steps. MT aptamer *in vitro*: 1.5 mM 2′-deoxyguanosine was titrated into 100 μM MT aptamer in solution in 20 steps. MT aptamer *in metabolo*: 1.5 mM 2′-deoxyguanosine was titrated into 86 μM MT aptamer solution in 25 steps. For the titration experiments in presence of guanosine, 50 μM guanosine was added to the buffer containing 50 mM potassium hydrogen phosphate, 50 mM potassium chloride, 5 mM magnesium chloride, pH 6.2.

ITC-Origin 7.0 was used to analyze ITC raw data to correct the dilution heat of the compounds and to model a non-linear regression employing a 'one set of sites' binding model. For the WT:guanosine:2'-deoxyguanosine titration experiments, a 'competitive binding' model was used to model the experimental data.

Aptamer and ligand concentrations were determined by UV absorption with NanoDrop 1000 spectrophotometer (Thermo Fisher Scientific) using the respective molar extinction coefficients (WT aptamer: ϵ_{260} = 635 000 l/(M cm), MT aptamer: ϵ_{260} = 598 000 l/(M cm), 2′-dG: ϵ_{254} = 13 300 l/(M cm), guanosine: ϵ_{260} = 11 800 l/(M cm)).

β-Galactosidase reporter assay

Plasmid constructs were derived from pDG_xpt_wt (20), in which the *xpt* 5′-untranslated region is fused directly upstream of the *lacZ* reporter gene. The *xpt* aptamer domain was replaced by the WT and MT aptamers by PCR mutagenesis and cloning using BamHI and EcoRI restriction sites (plasmid sequences are available upon request). The sequences used in the assay are depicted in Supplementary Table S1. The P1 stem of the *xpt* aptamer was not changed to ensure correct interaction between the aptamer domain and the expression platform. Mutations of the *M. florum* P1 stem were considered non-invasive according to the findings of Batey *et al.*, who demonstrated that a 2′-dG aptamer comprising the *xpt* P1 stem has nearly the same K_D to 2′-dG as the wild-type (68 nM versus 60 nM) (12). Plasmids were integrated into *B. subtilis* 168 genome at the *amyE* locus (20). *B. subtilis* cultures were grown for 14 h with shaking at 150 rpm at 37°C in CSK minimal media containing 0.5% (w/v) glucose, 25 mM $(NH_4)_2SO_4$, 70 mM K_2HPO_4, 25 mM KH_2PO_4, 22 mg/l (NH_4)FeIII-citrate, 0.5 mM $MgSO_4$, 10 μM $MnSO_4$, 0.8% K^+-glutamate, 5 μg/ml chloramphenicol, 50 μg/ml L-tryptophan, 0.2% Na^+-succinate (21). 2′-Deoxyguanosine was added at a final concentration of 0.5 mg/ml. Cultures were diluted to an OD_{600} of 0.03 and grown to a final OD_{600} of 0.5. β-Galactosidase activities were determined as described (22). Three independent cultures were measured in parallel. The measurements were repeated at least twice.

RESULTS

β-Galactosidase reporter gene assay of WT and MT aptamer

For the investigation of biological functionality of both aptamers, we analyzed whether the two 2′-dG aptamer domains (WT and MT) of *M. florum* can act as ligand-sensing domains in the *xpt* riboswitch in its host *B. subtilis*. We chose the *B. subtilis xpt* riboswitch because its aptamer domain is very similar to the 2′-dG aptamer (23). The ability to regulate gene expression of both, the WT and MT aptamer was tested in a β-galactosidase assay (Figure 2). In addition, a 2′-dG aptamer mutated at position C74, the specificity-generating position for ligand binding in all purine riboswitches containing guanine or its derivatives as ligand, was analyzed as a negative control. Upon addition of 2′-dG, β-galactosidase expression is repressed. The C74A mutation in the negative control leads to a complete loss of repression since ligand binding is prevented. Interestingly, although the MT aptamer has a functional ligand binding pocket, it fails to repress reporter gene expression, demonstrating its lack of function *in vivo*. Addition of high concentration of Mg^{2+} slightly restores the *in vivo* activity of the riboswitch with the MT aptamer domain (Supplementary Figure S1) which is in accordance with the observation of a Mg^{2+}-dependent ligand binding of this variant. At 5 mM Mg^{2+}, the MT aptamer showed a 20 ± 4% decrease in β-galactosidase activity in comparison to the β-galactosidase activity at 0.5 mM Mg^{2+}, but gene regulation of the MT riboswitch was low compared to the WT riboswitch (>90% reduction in β-galactosidase activity). β-Galactosidase activity was unaffected by additional Mg^{2+} for the WT and C74A aptamers. The biological assay demonstrates the sensitivity of the naturally evolved 2′-dG aptamer towards sequence modifications remote of the binding pocket *in vivo*.

Comparison of WT and MT aptamer binding to 2′-dG *in vitro* and in-cell extract

For direct comparison of the ligand binding behavior of both RNA aptamers, the WT aptamer was labeled with ^{15}N-uridine and the MT aptamer with ^{15}N-guanosine. This discriminative labelling permitted us to perform NMR experiments with one sample containing both aptamers under identical conditions. Upon binding of 2′-dG, both aptamers undergo conformational changes resulting in additional peaks in the imino proton region, which serve as ligand binding reporter signals (Figure 3A, G25 and U75). As a positive control we first carried out a ^{1}H,^{15}N-correlated BEST-TROSY experiment with 75 μM ^{15}N-uridine labeled wild-type (WT), 75 μM ^{15}N-guanine labeled MT aptamer, 300 μM 2′-dG and 5 mM Mg^{2+} in standard NMR buffer. The recorded spectrum revealed intact secondary and tertiary structure formation and particularly 2′-dG binding for both, WT and MT aptamer (Figure 3A). We then tested structure formation and 2′-dG binding competence in *B. subtilis* cell extract for identical amounts of RNA, ligand and Mg^{2+}. The RNA:ligand:Mg^{2+}-complex was mixed with *B. subtilis* cell extract and a ^{1}H,^{15}N-correlated BEST-TROSY experiment was performed immediately after. In this cellular environment, the WT aptamer exhibited stable secondary structure formation and ligand binding (Figure 3B). However, the spectrum of the MT construct lacked the reporter signal for 2′-dG binding (G25), whereas most of the reporter signals for correct secondary structure formation remained detectable (Figure 3B). The presence of a vast number of different cellular compounds drastically decreases the signal-to-noise ratio and also induces differential sensitivity of exchangeable imino sites to exchange broadening, thus weaker signals could not be detected. Increase of RNA (150 μM), 2′-dG (600 μM) and Mg^{2+} (10 mM) concentration recovered ligand binding for the MT aptamer in-cell extract (Figure 3C), proving the structural integrity of both aptamers under in-cell conditions. Comparison of the 1D slices for the labeled peaks illustrates the threshold of detection (Figure 3B and C).

Since *B. subtilis* extract reflects a near-native physiological environment containing intact macromolecules, in particular also ribonucleases and metabolites, the externally added RNA aptamers are degraded. In order to exclude differential stabilities of both RNA aptamers, pseudo 3D NMR experiments (Figure 3C) were analyzed in a time-resolved manner. The black and light gray bars in Supplementary Figure S2 depict the time-dependent decrease of signal integrals of WT and the MT aptamer, respectively. After 19 h, the peak integrals for both RNA aptamers were reduced by 20%. Taken into account the fluctuation of the noise peaks (dark grey bars), the progression of peak integral decrease was similar for both RNA constructs, indicating that there is no significant stability difference between them.

In order to further confine the molecular content of the *B. subtilis* cell extract and to exclude the aspect of degradation by endogenous RNases, we prepared a macromolecule-free metabolite extract of *B. subtilis* cells. To compare ligand binding of WT and MT aptamer in this reduced environment, a sample containing both aptamers, ligand and Mg^{2+} (75 μM ^{15}N-guanosine-labeled MT aptamer, 75 μM ^{15}N-uridine-labeled WT, 300 μM 2′-dG, 5 mM Mg^{2+} in *B. subtilis* metabolite extract) was prepared. The ^{1}H, ^{15}N-correlated HSQC spectrum of this sample (Figure 4B) reproduced the result of the NMR experiments carried out in the cell extract. The WT aptamer formed stable secondary and tertiary structure and was able to bind ligand *in vitro* and in metabolite extract. For the MT aptamer, however, the ligand binding reporter signal G25 was not detected, although formation of stable secondary structure could be observed. Addition of 5 mM Mg^{2+} could not recover the ligand binding reporter signal of the MT aptamer (data not shown). Only after increase of 2′-dG concentration to 600 μM (RNA:ligand = 1:4) at 5 mM Mg^{2+}, 2′-dG binding of the MT construct was recovered (Figure 4B).

2′-dG binding to WT is significantly affected by presence of endogenous metabolites

The NMR results indicate that intensities of the ligand binding reporter signal decrease in the presence of metabolites. In case of the MT aptamer, the reporter signal of G25 was too weak to be detectable under given conditions (Figure 4B). However, NMR data alone are not sufficient to conclude whether the weakening of the ligand binding reporter signals was due to interactions between metabolites

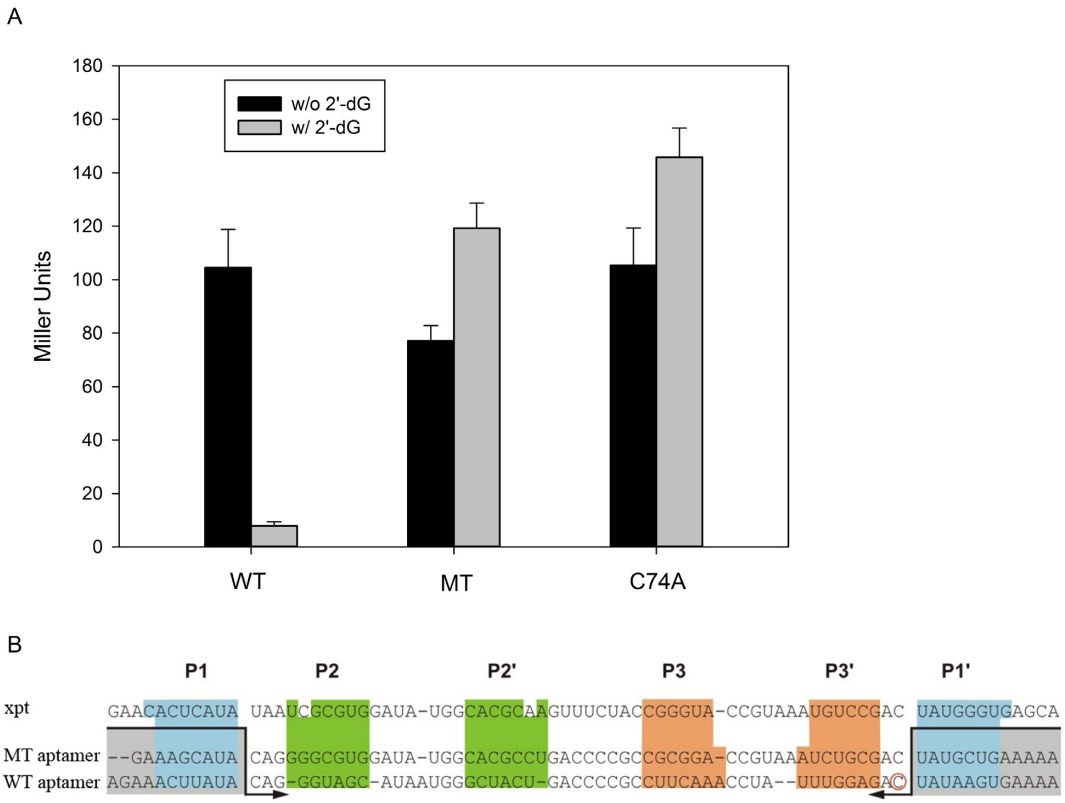

Figure 2. β-Galactosidase reporter gene assay of several aptamer domains embedded in the *xpt* riboswitch of *B. subtilis* fused to a *lacZ* gene. (**A**) Bars report β-galactosidase expression in Miller Units depending on aptamer constructs in absence (black) and presence (gray) of 0.5 mg/ml 2′-deoxyguanosine (2′-dG). WT is short for 2′-dG riboswitch aptamer domain, the MT aptamer was introduced in Figure 1, mutation C74A is not capable of ligand binding. Shown are the mean values of three independently measured cultures including the standard error mean values. The measurements were repeated at least twice. (30). (**B**) Aptamer sequences analysed by β-galactosidase assay. Colored boxes show helical domains of the aptamers, forming the stems P1 to P3 of the secondary structure. For MT and WT aptamer, P1 and P1' sequence of *xpt* aptamer of *B. subtilis* were used as indicated by arrows and grey boxes. P1 is only marginally involved in ligand binding but is crucial for expression platform interaction. Circled in red is the position C74 which is altered to A in the 2′-dG C74A construct.

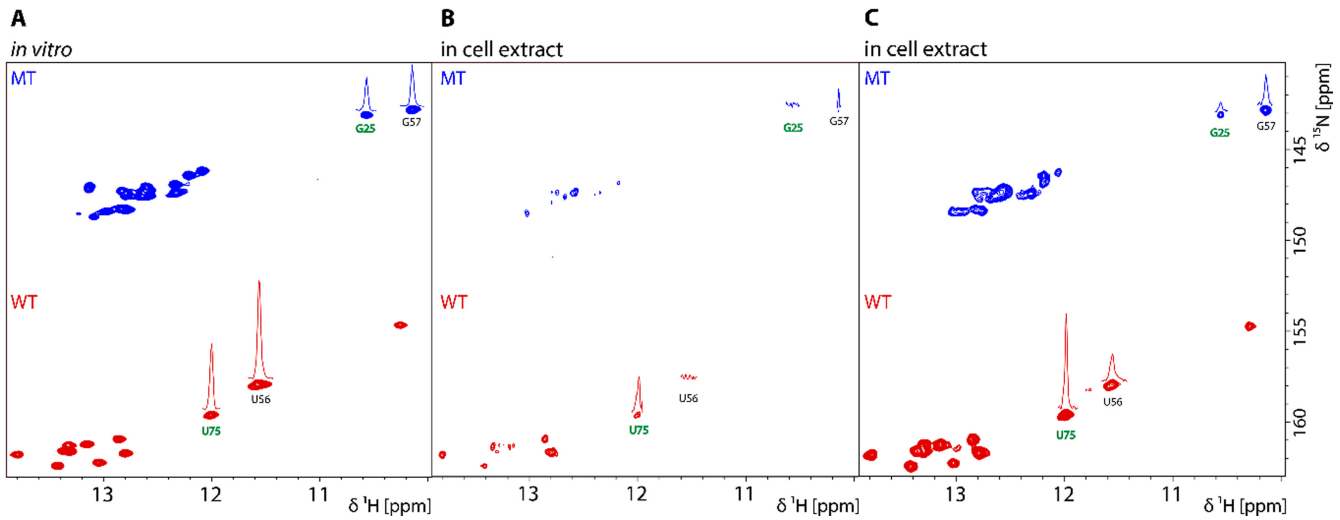

Figure 3. Ligand binding of ^{15}N-guanosine-labeled MT aptamer (blue peaks) and ^{15}N-uridine-labeled WT (red peaks) were analyzed by ^{1}H, ^{15}N-correlated NMR experiments *in vitro* (**A**) and in *B. subtilis* cell extract (**B**, **C**). The differential labelling pattern of WT and the MT aptamer allowed us to distinguish signals, even though they were present in a single sample. (A) *In vitro* conditions for both aptamers, WT (75 μM) and MT aptamer (75 μM), ligand binding reporter signals were detected (annotated in green). (B) Once the identical concentrations of RNA (75 μM of each aptamer), cognate ligand (300 μM 2'-deoxyguanosine) and $MgCl_2$ (5 mM) were taken into in-cell-like environment, G25 the reporter signal for ligand binding of the MT aptamer could not be detected. In addition, other signals including U56 disappeared. (C) At [RNA] = 300 μM, [Ligand] = 600 μM and [$MgCl_2$] = 10 mM the ligand binding reporter signal of the MT construct was recovered. Uridine 75, the prominent ligand binding reporter signal of WT, could be detected throughout all tested conditions.

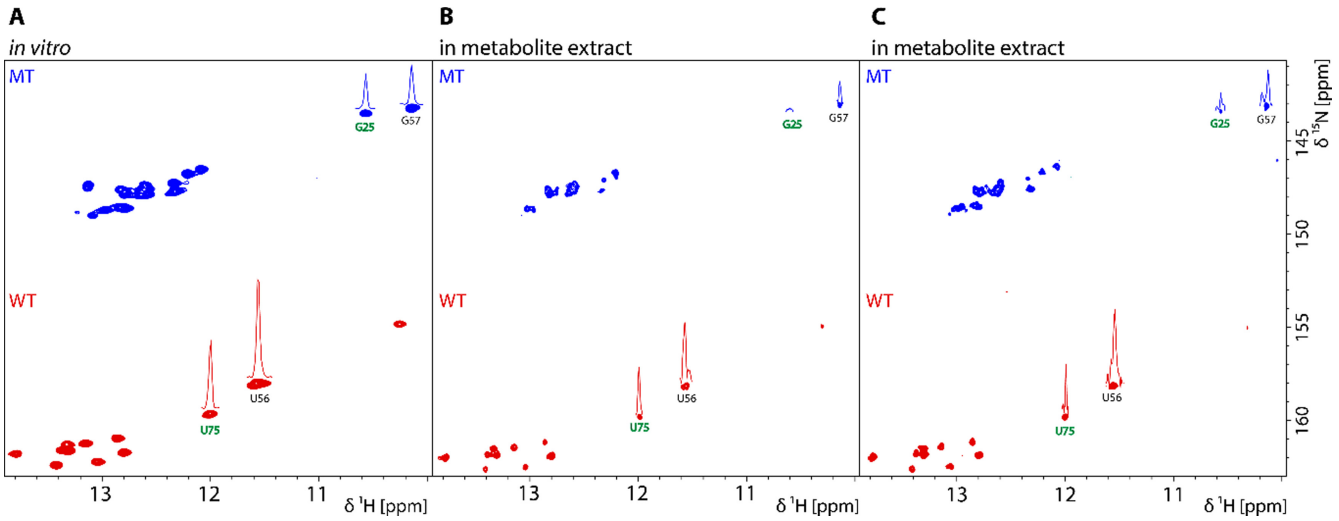

Figure 4. Ligand binding of ^{15}N-guanosine-labeled MT aptamer (blue peaks) and ^{15}N-uridine-labeled WT (red peaks) were analyzed by NMR *in vitro* (**A**) and in *B. subtilis* metabolite extract (**B** and **C**). The differential labelling pattern of WT (red peaks) and MT aptamer (blue peaks) allowed us to distinguish signals from both aptamers, even though they were combined in a single sample. (A) *In vitro* for both aptamers, WT (75 μM) and MT aptamer (75 μM), the ligand binding reporter signals were detectable. (B) Once the identical concentrations of RNA (75 μM of each aptamer), cognate ligand (300 μM 2′-deoxyguanosine) and $MgCl_2$ (5 mM) were taken into metabolite extract, the ligand binding reporter signal of the MT aptamer could no longer be detected. (C) Upon increase of ligand concentration to 600 μM the ligand binding reporter signal of the MT construct could be recovered.

and the aptamers or simply the result of lower signal-to-noise ratio, caused by the presence of a wide range of small molecules. Therefore, we determined 2′-dG binding affinity of the aptamers by ITC experiments *in vitro* and in-cell-like conditions (Figure 5 and Table 1). In both cases, metabolites from cell extract bind to the aptamers, and titrations of resulting complexes with 2′-dG mimic a 'competition binding assay' (24,25), leading to altered thermodynamic parameters of titrations in comparison to *in vitro* experiments (Table 1). For the WT aptamers, we observe an usual ligand competition situation, where both, K_D and ΔH significantly differ in both conditions (K_D values 0.15 and 1.74 μM, ΔH values −24.2 and −9.0 kCal/mol, *in vitro* and *in metabolo*, respectively), indicating binding of metabolites to WT aptamer with K_D values in low micromolar range. In contrast, the MT sequence has a relatively high K_D value of 13.5 μM *in vitro* that remains almost unchanged in metabolite extract ($K_D = 25.3$ μM), whereas ΔH values are still varied (−22.5 and −15.2 kcal/mol, *in vitro* and *in metabolo*, respectively). In this case metabolites do not bind the MT aptamer in specific manner, rather bind WT due to their high concentration in the cell extract. Consequentially, the 2′-dG—as the most affine component—can still compete them from MT aptamer, but changes in the apparent thermodynamic parameters (by analysis of the ITC curves with 'single set of sites' model) for 2′-dG:MT interaction *in vitro* and *in metabolo* are not as pronounced as for 2′-dG:WT interaction.

Endogenous metabolite binds to WT aptamer

2′-dG was simultaneously titrated to ^{15}N-guanine-uridine-labeled WT and ^{15}N-guanine-uridine-labeled MT aptamer under two different conditions, in NMR-buffer and in *B. subtilis* metabolite extract. Here, we utilize the imino proton of 2′-dG, which exchanges rapidly with solvent water in the unbound state, but is detectable at $\delta^1H = 12.98$ ppm when the RNA:ligand complex is formed (Figure 6 A inlet). Figure 6A–D depict the process of titration for each RNA aptamer at each condition by following the increase of the imino proton signal at 12.98 ppm, which arises when a Watson–Crick base pair between C74 of the RNA aptamer and 2′-dG is formed (Figure 6 A). Under both conditions, *in vitro* and *in metabolo*, an increase of the signal of bound ligand could be detected for WT and the MT aptamer during titration. Comparison of both *in vitro* titrations reveals for WT a saturation with no further significant increase of the imino proton signal at 0.8 equivalents of ligand, whereas for the MT aptamer a continuous increase of the binding signal was observed up to the final titration point at 2.0 equivalents of 2′-dG (Figure 6A and C), in line with the differences in affinity determined in ITC experiments. In contrast, both RNA aptamers reach saturation at 1.0 equivalents of ligand titration in the presence of metabolites (Figure 6B and D). Strikingly, WT in metabolite extract displays a distinct imino proton peak at a different position than the 2′-dG reporter signal, even in the absence of 2′-deoxyguanosine (Figure 6B, blue spectrum). This initial binding signal, indicating specific interaction between components of the metabolic extract from *B. subtilis* and WT aptamer, first broadened and finally disappeared and the signal characteristic for binding to 2′-deoxyguanosine appeared, indicating displacement of the pre-bound metabolite.

The increasing integrals of the 2′-dG binding peak (Figure 6A–D) during titration were plotted against 2′-dG concentration. Monitoring the integrals of the binding peak for each construct under each condition, display the relative change in apparent affinity for WT and MT aptamer, respectively (Supplementary Figure S3). An accurate determination of dissociation constants is difficult to carry out,

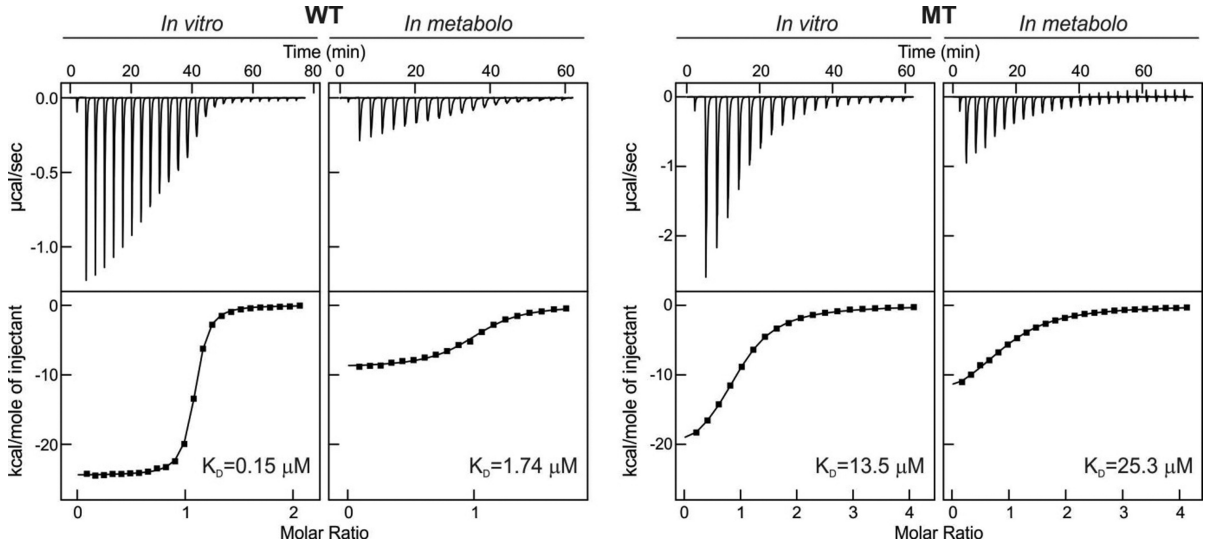

Figure 5. Interactions of WT and MT aptamers with 2′-deoxyguanosine *in vitro* and in *B. subtilis* metabolite extract (*In metabolo*). Top panel displays the raw heat per injection, the lower panel displays the integrated heat per titration over molar ratio (aptamer:ligand) with correction to heat of dilution. K_D values determined by 'one set of sites' binding model for each aptamer are given for each experiment (more detailed information is given in Table 1).

Table 1. Thermodynamic parameters of interactions between WT and MT aptamers with their ligands *in vitro* and *in metabolo*

	ΔH (kcal mol^{-1})	ΔS (cal mol^{-1} K^{-1})	$-T^*\Delta S$ (kcal mol^{-1})	ΔG (kcal mol^{-1})	$K_A \times 10^6$ (M^{-1})	K_D (µM)	*N* sites
Aptamer WT, titration with 2′-dG							
The data analysed by 'one binding site' model							
In vitro	−24.2 ± 0.0*	−52.1	+15.16	−9.08	6.48 ± 0.21	0.15	1.05 ± 0.00
In metabolo	−9.0 ± 0.1	−4.47	+1.30	−7.67	0.57 ± 0.01	1.74	1.00 ± 0.01
In vitro, guanosine-saturated, the data analysed by 'one binding site' model							
	−5.6 ± 0.2	+7.7	−2.24	−7.79	0.70 ± 0.05	1.42	0.93 ± 0.02
In vitro, guanosine-saturated, the data analysed by 'competitive binding' model with the parameters of WT:guanosine interaction taken from experiment below							
	−22.1 ± 0.2	na	na	na	26.2 ± 1.4	0.04	0.94 ± 0.02
Aptamer WT, titration with guanosine							
In vitro	−16.4 ± 0.0	−28.7	+8.35	−8.00	1.01 ± 0.03	0.99	1.18 ± 0.00
Aptamer MT, titration with 2′dG							
In vitro	−22.5±0.2	−55.0	+16.00	−6.49	0.074 ± 0.0	13.5	0.92 ± 0.01
In metabolo	−15.2 ± 0.3	−31.0	+9.02	−6.14	0.040 ± 0.0	25.3	0.95 ± 0.01

*The values after '±' sign indicates fitting error for selected parameter; overall experimental error for the ITC data presented in the table does not exceed 15%.

nevertheless, we could observe a significant decrease of the slope in the regression curve of WT *in metabolo* in comparison to WT *in vitro* (Supplementary Figure S3A). Consequently, the apparent ligand binding affinity is negatively affected by the presence of metabolites, which was not observed for the MT aptamer as the regression curves of *in vitro* and in metabolo resemble each other (Supplementary Figure S3).

In addition to the ^{14}N-edited imino proton signal, which arises from ligands but not from the ^{15}N-labeled RNA and demonstrates aptamer–ligand complex formation, we also monitored alterations in the secondary structure of each RNA–aptamer under each condition during ligand titration. Both RNA-constructs, WT and MT aptamer respectively, were uniformly ^{15}N-GU-labeled, hence all imino proton signals in a ^{15}N-edited 1D spectrum illustrate the secondary structure of the aptamers. Dramatic structural changes were observed for WT *in vitro*, MT aptamer *in vitro* and MT aptamer *in metabolo* (Figure 7A, C and D), each of those induced by complex formation with 2′-deoxyguanosine. The final spectra of each aptamer after titration were similar regardless of the condition the experiment was carried out in (comparing red spectrum in Figure 7A with B and C with D) showing that the same global fold is adopted by the RNA:ligand complex *in vitro* and *in metabolo*. However, apo-WT *in metabolo* adopted already a tertiary structure typically seen for the holo state in the absence of its cognate ligand 2′-dG, as the overall imino proton signal pattern remained unaltered throughout ligand titration (Figure 7 B). Furthermore, the U75 imino proton signal, reporter signal for ligand binding, is present for WT *in metabolo* before titration with 2′-dG, pointing towards a specific interaction between WT aptamer and an endogenous metabolite in the ligand binding pocket, in agreement with the titration data reported above.

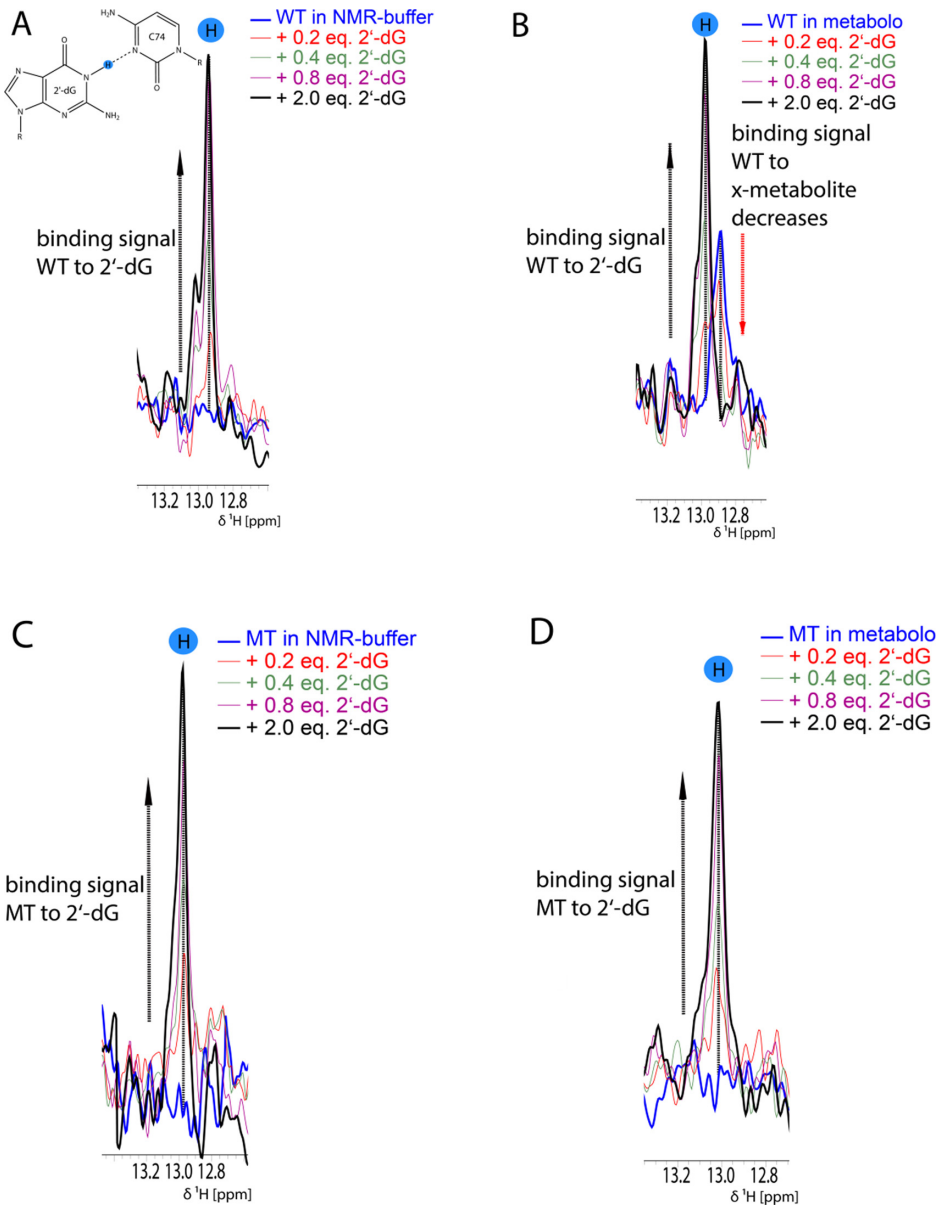

Figure 6. NMR titration of 2′-deoxyguanosine to ^{15}N-labeled WT and ^{15}N-labeled MT aptamer *in vitro* and *in metabolo* respectively. Overlay of ^{14}N-edited imino proton spectra of the RNA aptamer-2′-deoxyguanosine complex of WT in NMR-buffer (**A**), *in metabolo* (**B**), of MT aptamer in NMR-buffer (**C**) and *in metabolo* (**D**). All spectra were recorded at a 600 MHz spectrometer with 256 scans at $T = 291$ K. The imino proton signals marked with a blue circle are only detectable once a Watson–Crick base pair is formed between C74 of the RNA aptamer domain and the ligand 2′-deoxyguanosine (A). The black dotted arrows indicate the increase of this signal during titration. The spectra of WT *in metabolo* (B) shows an additional imino proton signal even before the first titration with 2′-deoxyguanosine (blue spectrum in B), which intensity decreases upon subsequent 2′-dG titration (indicated by red dotted arrow). Two binding peaks detectable for WT point at binding heterogeneity, as also previously observed for residue A34 (31).

Identification of WT-binding metabolite

For the identification of the exact WT-binding metabolite, titration experiments were carried out with several metabolites. Unlabeled metabolites were titrated to ^{15}N-labeled WT-aptamer and a ^{14}N-edited 1D spectrum was recorded after each titration. An imino proton signal in the ^{14}N-edited 1D spectra could only be observed after titration with 200 μM guanosine (Figure 8A). For the other nine tested metabolites (inosine, 2′-deoxyinosine, NAD, imidazole, histidine, uridine, hypoxanthine, GTP and dGMP) no binding signal could be detected. As negative and positive controls, the 1D traces of WT only and WT in complex with 2′-deoxyguanosine were overlaid (Figure 8A). The similar chemical shift of both binding peaks of 2′-dG and guanosine indicates the occupation of a similar binding site on the aptamer, hence both metabolites compete for the ligand binding pocket.

Overlaying the 1D trace of free guanosine (Figure 8C, thin solid line) onto the spectrum of metabolite extract (Figure 8C, thick solid line) revealed a peak in the *in metabolo* spectrum, which was assigned to H8 proton of guanosine. The small chemical shift difference, however, did not allow

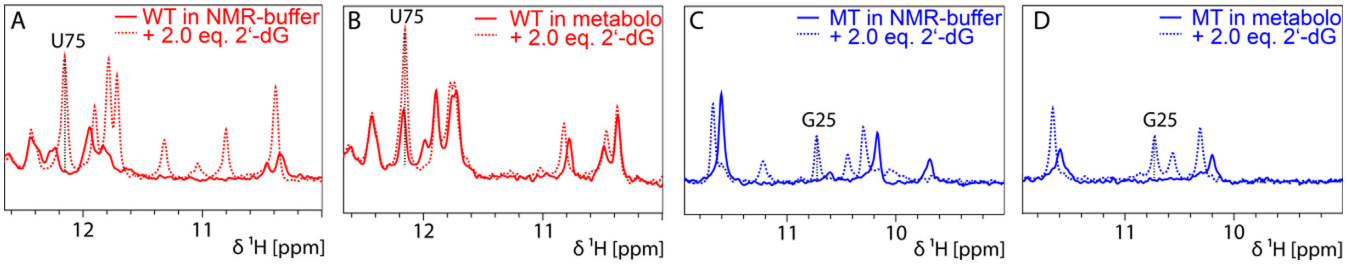

Figure 7. Comparison of secondary structure of WT and MT aptamer before and after ligand titration. Observing the ^{15}N-edited imino proton spectra of the uniformly ^{15}N-GU-labeled RNA aptamers during titration with unlabeled 2′-deoxyguanosine exhibits secondary structural changes upon ligand binding of WT *in vitro* (**A**), WT *in metabolo* (**B**), MT aptamer *in vitro* (**C**) and MT aptamer *in metabolo* (**D**). In all cases, the spectrum with bold lines depicts the state before beginning of titration and the dottet spectrum after final titration. The respective ligand binding reporter signals are marked with dotted black lines with the appropriate assignment.

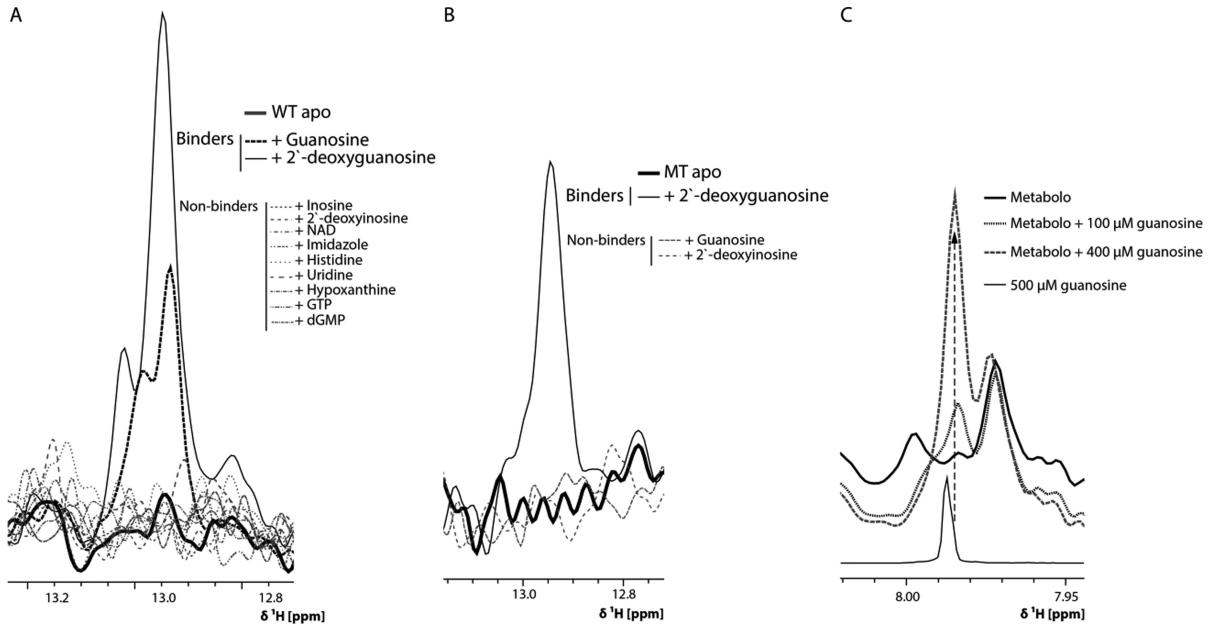

Figure 8. (**A**) Titration of unlabeled metabolites to 150 μM ^{15}N-labeled WT-aptamer. In order to study the binding capacity of each tested compound ^{14}N-edited 1D-spectra have been recorded before starting titration (WT only) and after each titration. Only for two compounds binding peaks could be detected, one of them being the cognate ligand (2′-deoxyguanosine) and the other one Guanosine. (**B**) Titration of unlabeled metabolites to 150 μM ^{15}N-labeled MT-aptamer. In order to study the binding capacity of each tested compound ^{14}N-edited 1D-spectrum have been recorded before starting titration (MT aptamer only) and after each titration. In case of the MT aptamer there was only one binder, the cognate ligand 2′-deoxyguanosine (300 μM). For both guanosine (400 μM) and 2′-deoxyinosine (400 μM) no binding signal were detectable. (**C**) Guanosine titration to *B. subtilis* metabolite extract. ^{1}H-1D spectra were recorded of metabolite extract only (black solid line), after titration of 100 μM guanosine (dotted line) and in presence of 400 μM guanosine (dashed line). As a reference the 1D trace of guanosine alone has been overlayed (thin black line). The upcoming guanosine peak (dotted arrow) can be backtracked to locate the guanosine peak *in metabolo* only.

an unambiguous assignment. To verify that conclusion, increasing amounts of guanosine were titrated to the metabolite extract. In fact, the peak with increasing peak intensity during titration originates at the peak with the chemical shift at around 7.98 ppm. We attribute the small chemical shift difference of 0.01 ppm between free guanosine and *in metabolo* to slightly altered environment.

NMR results indicate interaction between the WT aptamer and the non-cognate ligand guanosine. To compare the binding affinity of cognate ligand and non-cognate ligand ITC experiments have been performed. The ITC trace in Figure 9A illustrates the interaction between guanosine and WT aptamer. The K_D value of 0.99 μM is 6-fold higher than that for the WT to 2′-dG interaction. We then further tested competition between guanosine and 2′-dG to WT aptamer binding *in vitro* by ITC. We saturated WT aptamer with guanosine (molar ratio 1:5) and performed titration of this sample with 0.5 mM 2′-dG solution in the same buffer. This experiment resulted in a competition curve (Figure 9B), from which we could determine thermodynamic parameters of WT:2′-dG interaction with corresponding analysis (Competitive binding model). The parameters presented in Table 1 are identical to those observed in the direct ITC experiment for *in vitro* titration of WT aptamer with 2′-dG (Figure 5 and Table 1), indicating correctness of the competition model. Analysis of the ITC data for 2′-dG titration to WT aptamer with incomplete guanosine saturation confirms this conclusion (Supplementary Figure

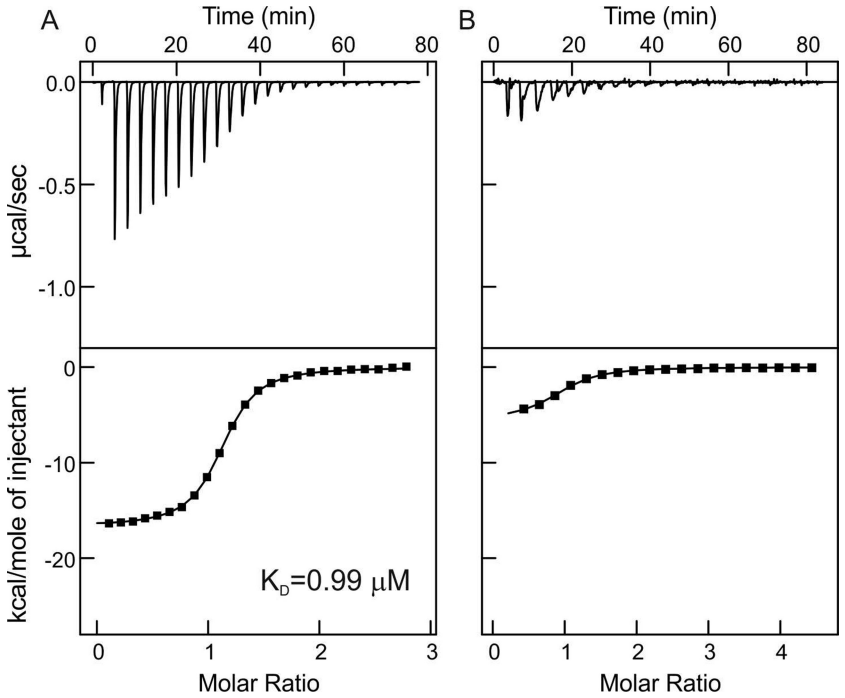

Figure 9. Interactions of WT aptamer with guanosine (**A**) and with 2′-deoxyguanosine in presence of guanosine (**B**). When WT is pre-bound to guanosine (B), ITC trace shows a competition experiment. Using a 'competitive binding' model and thermodynamic parameters of WT:guanosine interaction determined from (A), we were able to quantitatively reconstitute parameters of WT:2′-deoxyguanosine interaction *in vitro* (Figure 5A and Table 1). Top panels display the raw heat per injection, the lower panels display the integrated heat per titration over molar ratio (aptamer:ligand) with correction to heat of dilution.

S4 and Table S2). Additionally, similarity between thermodynamic parameters of WT aptamer interaction with 2′-dG in presence of guanosine *in vitro* and that for WT:2′-dG interaction *in metabolo* indicates that guanosine is the main natural competitor of 2′dG in-cells.

DISCUSSION

In-cell NMR is a powerful method to validate *in vitro* structural data of functional biomolecules. Factors including ionic composition, presence of macromolecules as potential specific or unspecific binding partners, molecular crowding and the abundance of endogenous compounds can affect the conformation, dynamics and particularly the intermolecular interactions. Hence, *in vitro* NMR data could diverge from in-cell NMR results. In this work, we tested whether in-cell conditions can alter riboswitch binding behavior by investigation of binding to an aptamer domain.

Instead of injecting exogenous biomolecules into a cell, we prepared cell lysates and reconstituted our compound in it, thus bringing the molecule of interest into an in-cell-like environment. Under such conditions, the characteristics like molecular crowding or composition of endogenous compounds are maintained, whereas the line-width of the spectra is significantly decreased (26). This set-up allowed us to prepare and detect RNA concentrations between 75 and 150 µM and metabolite concentrations up to 600 µM. RNA concentrations were mostly limited by solubility of the titrated metabolites, but in general, sample preparations in cell extracts faces no inherent concentration limit.

Importantly, our approach also facilitates the simultaneous observation of NMR signals of differentially labeled RNA aptamers in the very same sample. In principle, up to 4–6 different RNAs could be observed at the same time if uniform differential ^{13}C-labeling and ^{15}N-labeling of each nucleotides was applied, and segmental labeling would even increase this scope.

The change in the peripheral elements of the riboswitch impacted not only the affinity to the cognate ligand, but also the binding capabilities of the riboswitch to ligands similar to 2′-dG. In the MT aptamer domain we do not observe affinity to guanosine, which we can detect for the WT aptamer. The ITC results nicely correlated with the outcome of NMR titration experiments, in which the apparent ligand binding affinity of only the WT aptamer was negatively affected by the presence of endogenous metabolites (Figure 5, Table 1 and Figure 6). Analysis of the ITC results explicitly shows that the only model, correctly describing all titration experiments, is the model of competitive binding. According to that, WT and MT aptamers *in metabolo* are pre-bound to the cell metabolites—proportionally to their affinity to either aptamers and relative concentrations in cells. An unbiased screening with six purine analogs and four indifferent metabolites by NMR (Figure 8) led us to conclude that guanosine, a higher abundant derivate of the cognate ligand 2′-dG, could compete for the ligand binding pocket, thus interfering with the binding of 2′-dG and lowering the apparent affinity between aptamer and cognate ligand (Figure 9) (27). This observation is in line with the fact that there is a crystal structure of WT aptamer domain in com-

plex with guanosine in addition to the 2′-dG-bound X-ray structure (28). In the X-ray structure, the additional 2′-OH of guanosine group leads to a less compact binding pocket, most drastically illustrated by the change of conformation of nucleotide C49. In the 2′-dG-bound structure, the base moiety of C49 is turned into the binding pocket, stacking on C48 and the C49 phosphate group is located close proximity to the deoxyribose ring of the ligand. For guanosine, the ribose orientation is slightly altered and the phosphate group of C49 is pushed away from the ligand, along with a complete swing-out of the base into the solution. Indeed, our ITC results show that the K_D values for WT aptamer to 2′-dG are 5-fold lower than for guanosine.

For MT aptamer, there is no such specificity to the guanine-based nucleosides, therefore, a pool of metabolites could unspecifically bind to the MT aptamer in cells due to high concentrations of each metabolite. Consequently, displacement by 2′-dG in this case is much less efficient (almost no K_D difference for 2′-dG:MT interaction *in vitro* and *in metabolo*) but still exist (significant ΔH difference for 2′-dG:MT interaction *in vitro* and *in metabolo*).

The existence of endogenous binding-competent compounds alters the regulation range of the riboswitch deviating from the expected range based on *in vitro* data alone. Concentrations of 2′-dG in *E. coli* have been published. These differ, however, from each other dependent on used strain, growth condition and the utilized extraction protocol. In *E. coli* the 2′-dG concentration is 4-fold higher than the guanosine concentration (29). By NMR spectroscopy we could determine the guanosine concentration (0.9 μM) in *B. subtilis* metabolite extract, hence the estimated deoxyguanosine concentration would yield 0.2 μM. Lower abundance of 2′-dG is compensated by its higher binding affinity to WT aptamer. The structural similarity of WT *in metabolo* and WT in complex with 2′-dG and the fact that G binds also to the full-length 2′-dG riboswitch confirm that endogenous guanosine has an impact on 2′-dG regulation. As observed in single-round *in vitro* transcription assays, guanosine in fact enhances premature transcription termination by a factor of 1.6, similar to guanine (factor 1.9), compared to a factor of 2.5 at 25 μM 2′-dG.

Our β-galactosidase reporter gene assays showed that addition of 1.8 mM 2′-dG results in approximately 10-fold reduction of reporter gene expression in the presence of endogenous guanosine, suggesting a higher riboswitch efficiency *in vivo* compared to *in vitro.* In this light, binding of endogenous guanosine to the aptamer domain of the 2′-dG riboswitch constitutes but a basal offset of riboswitch activity, probably not even affecting the 21% intrinsically terminated mRNA molecules observed *in vitro* in the absence of any ligand (7).

Synthetic riboswitches evolved via the SELEX process are well characterized with respect to affinity and selectivity to their target ligand *in vitro*. Once applied as gene regulators, however, it is observed that some of the synthetic riboswitches does not function as expected (6). Here we presented a particular example where *in vitro* data differ from data obtained under in-cell experimental setups. Hence, focusing only on affinity of the preferred ligand to a RNA aptamer under *in vitro* conditions is not sufficient, but mimicking metabolome in addition could reveal crucial insight into regulation and functionality of riboswitches.

SUPPLEMENTARY DATA

Supplementary Data are available at NAR Online.

ACKNOWLEDGEMENTS

We thank Christian Richter und Boris Fürtig for help with NMR experiments. We thank Katharina Weickhmann and Jens Wöhnert for help with and access to the ITC instrument.

FUNDING

DFB: CRC902 (‘Principles of RNA-based regulation’) and EXC115: macromolecular complexes; State of Hessen (to B.M.R.Z.); SFB 1177 ‘Molecular and Functional Characterization of Selective Autophagy’, Germany (to V.V.R.). Funding for open access charge: DFG.
Conflict of interest statement. None declared.

REFERENCES

1. Nudler,E. and Mironov,A.S. (2004) The riboswitch control of bacterial metabolism. *Trends Biochem. Sci.*, **29**, 11–17.
2. Tucker,B.J. and Breaker,R.R. (2005) Riboswitches as versatile gene control elements. *Curr. Opin. Struct. Biol.*, **15**, 342–348.
3. Wickiser,J.K., Winkler,W.C., Breaker,R.R. and Crothers,D.M. (2005) The speed of RNA transcription and metabolite binding kinetics operate an FMN riboswitch. *Mol. Cell*, **18**, 49–60.
4. Tuerk,C. and Gold,L. (1990) Systematic evolution of ligands by exponential enrichment: RNA ligands to bacteriophage T4 DNA polymerase. *Science*, **249**, 505–510.
5. Ellington,A.D. and Szostak,J.W. (1990) In vitro selection of RNA molecules that bind specific ligands. *Nature*, **346**, 818–822.
6. Wittmann,A. and Suess,B. (2012) Engineered riboswitches: expanding researchers’ toolbox with synthetic RNA regulators. *FEBS Lett.*, **586**, 2076–2083.
7. Kim,J.N., Roth,A. and Breaker,R.R. (2007) Guanine riboswitch variants from Mesoplasma florum selectively recognize 2′-deoxyguanosine. *Proc. Natl. Acad. Sci. U.S.A.*, **104**, 16092–16097.
8. Wacker,A., Buck,J., Mathieu,D., Richter,C., Wöhnert,J. and Schwalbe,H. (2011) Structure and dynamics of the deoxyguanosine-sensing riboswitch studied by NMR-spectroscopy. *Nucleic Acids Res.*, **39**, 6802–6812.
9. Thelander,L. and Reichard,P. (1979) Reduction of ribonucleotides. *Ann. Rev. Biochem.*, **48**, 133–158.
10. Kolberg,M., Strand,K.R., Graff,P. and Andersson,K.K. (2004) Structure, function, and mechanism of ribonucleotide reductases. *Biochim. Biophys. Acta - Proteins Proteomics*, **1699**, 1–34.
11. Noeske,J., Richter,C., Grundl,M.A., Nasiri,H.R., Schwalbe,H. and Wöhnert,J. (2005) An intermolecular base triple as the basis of ligand specificity and affinity in the guanine- and adenine-sensing riboswitch RNAs. *Proc. Natl. Acad. Sci. U.S.A.*, **102**, 1372–1377.
12. Edwards,A.L. and Batey,R.T. (2009) A Structural Basis for the Recognition of 2′-Deoxyguanosine by the Purine Riboswitch. *J. Mol. Biol.*, **385**, 938–948.
13. Selenko,P., Serber,Z., Gadea,B., Ruderman,J. and Wagner,G. (2006) Quantitative NMR analysis of the protein G B1 domain in Xenopus laevis egg extracts and intact oocytes. *Proc. Natl. Acad. Sci. U.S.A.*, **103**, 11904–11909.
14. Serber,Z., Selenko,P., Hänsel,R., Reckel,S., Löhr,F., Ferrell,J.E., Wagner,G. and Dötsch,V. (2006) Investigating macromolecules inside cultured and injected cells by in-cell NMR spectroscopy. *Nat. Protoc.*, **1**, 2701–2709.
15. Stoldt,M., Wöhnert,J., Görlach,M. and Brown,L.R. (1998) The NMR structure of Escherichia coli ribosomal protein L25 shows

homology to general stress proteins and glutaminyl-tRNA synthetases. *EMBO J.*, **17**, 6377–84.
16. Favier,A. and Brutscher,B. (2011) Recovering lost magnetization: polarization enhancement in biomolecular NMR. *J. Biomol. NMR*, **49**, 9–15.
17. Lescop,E., Kern,T. and Brutscher,B. (2010) Guidelines for the use of band-selective radiofrequency pulses in hetero-nuclear NMR: Example of longitudinal-relaxation-enhanced BEST-type 1H-15N correlation experiments. *J. Magn. Reson.*, **203**, 190–198.
18. Kupce,E. and Freeman,R. (1994) Wideband excitation with polychromatic pulses. *J. Magn. Reson. Ser. A*, **108**, 268–273.
19. Geen,H. and Freeman,R. (1991) Band-selective radiofrequency pulses. *J. Magn. Reson.*, **93**, 93–141.
20. Mandal,M., Boese,B., Barrick,J.E., Winkler,W.C. and Breaker,R.R. (2003) Riboswitches control fundamental biochemical pathways in Bacillus subtilis and other bacteria. *Cell*, **113**, 577–586.
21. Inacio,J.M., Costa,C., de Sá-Nogueira,I., Inácio,J.M., Costa,C. and de Sá-Nogueira,I. (2003) Distinct molecular mechanisms involved in carbon catabolite repression of the arabinose regulon in Bacillus subtilis. *Microbiology*, **149**, 2345–2355.
22. Miller,J.H. (1972) Experiments in molecular genetics. *Cold Spring Harb. Lab. Press. Cold Spring Harb. NY*, **433**, 352–355.
23. Mandal,M. and Breaker,R.R. (2004) Adenine riboswitches and gene activation by disruption of a transcription terminator. *Nat. Struct. Mol. Biol.*, **11**, 29–35.
24. Zhang,Y.L. and Zhang,Z.Y. (1998) Low-affinity binding determined by titration calorimetry using a high-affinity coupling ligand: a thermodynamic study of ligand binding to protein tyrosine phosphatase 1B. *Anal. Biochem.*, **261**, 139–148.
25. Velazquez-Campoy,A. and Freire,E. (2006) Isothermal titration calorimetry to determine association constants for high-affinity ligands. *Nat. Protoc.*, **1**, 186–91.
26. Hänsel,R., Foldynová-Trantírková,S., Löhr,F., Buck,J., Bongartz,E., Bamberg,E., Schwalbe,H., Dötsch,V. and Trantírek,L. (2009) Evaluation of parameters critical for observing nucleic acids inside living Xenopus laevis oocytes by in-cell NMR spectroscopy. *J. Am. Chem. Soc.*, **131**, 15761–15768.
27. Soga,T., Ohashi,Y., Ueno,Y., Naraoka,H., Tomita,M. and Nishioka,T. (2003) Quantitative metabolome analysis using capillary electrophoresis mass spectrometry. *J. Proteome Res.*, **2**, 488–494.
28. Pikovskaya,O., Polonskaia,A., Patel,D.J. and Serganov,A. (2011) Structural principles of nucleoside selectivity in a 2′-deoxyguanosine riboswitch. *Nat. Chem. Biol.*, **7**, 748–55.
29. Bennett,B.D., Kimball,E.H., Gao,M., Osterhout,R., Van Dien,S.J. and Rabinowitz,J.D. (2009) Absolute metabolite concentrations and implied enzyme active site occupancy in Escherichia coli. *Nat. Chem. Biol.*, **5**, 593–599.
30. Inacio,J.M., Costa,C., de Sá-Nogueira,I., Inácio,J.M., Costa,C. and de Sá-Nogueira,I. (2003) Distinct molecular mechanisms involved in carbon catabolite repression of the arabinose regulon in Bacillus subtilis. *Microbiology*, **149**, 2345–2355.
31. Wacker,A.B. (2012) PhD thesis, Johann Wolfgang Goethe University 2012.